



PAPER • OPEN ACCESS

Metabolic adaptation and fragility in healthy 3D *in vitro* skeletal muscle tissues exposed to chronic fatigue syndrome and Long COVID-19 sera

To cite this article: Sheeza Mughal et al 2025 Biofabrication 17 045006

View the article online for updates and enhancements.

You may also like

- Genetically programmable wearable devices for precision physiological and molecular monitoring
 Jin He, Mengdie Fu, Wenyue An et al.
- Engineering a microfluidic-assisted 3D bioprinting approach for the hierarchical control deposition and compartmentalisation of graded bioinks Federico Serpe, Lucia lafrate, Marco Bastioli et al.
- Embolization-on-a-chip: novel vascularized liver tumor model for evaluation of cellular and cytokine response to embolic agents Huu Tuan Nguyen, Zuzana Tirpakova, Arne Peirsman et al.

Biofabrication



OPEN ACCESS

RECEIVED

5 December 2024

REVISED

21 July 2025

ACCEPTED FOR PUBLICATION 31 July 2025

PUBLISHED

8 August 2025

Original content from this work may be used under the terms of the Creative Commons Attribution 4.0 licence.

Any further distribution of this work must maintain attribution to the author(s) and the title of the work, journal citation and DOI.



PAPER

Metabolic adaptation and fragility in healthy 3D *in vitro* skeletal muscle tissues exposed to chronic fatigue syndrome and Long COVID-19 sera

Sheeza Mughal^{1,8,*}, Félix Andújar-Sánchez^{2,3,4}, Maria Sabater-Arcis¹, Glória Garrabou^{2,3,4}, Joaquim Fernández-Solà³, Jose Alegre-Martin^{5,6}, Ramon Sanmartin-Sentañes^{5,6}, Jesús Castro-Marrero⁶, Anna Esteve-Codina^{7,8}, Eloi Casals^{7,8}, Juan M Fernández-Costa^{1,*} and Javier Ramón-Azcón^{1,9,*}

- ¹ Institute for Bioengineering of Catalonia (IBEC), Barcelona Institute of Science and Technology (BIST), Barcelona, Spain
- ² Inherited Metabolic Disorders and Muscular Diseases Research Group, Institut d'Investigacions Biomèdiques August Pi i Sunyer (IDIBAPS) and Faculty of Medicine and Health Sciences, University of Barcelona, 08036 Barcelona, Spain
- ³ Department of Internal Medicine, Hospital Clinic of Barcelona, 08036 Barcelona, Spain
- ⁴ CIBERER—Spanish Biomedical Research Centre in Rare Diseases, 28029 Madrid, Spain
- ⁵ Division of Rheumatology, Vall d'Hebron University Hospital, Universitat Autònoma de Barcelona, 08035 Barcelona, Spain
- ⁶ Unit of Research in ME/CFSyalgic Encephalomyelitis/Chronic Fatigue Syndrome and Long COVID, Division of Rheumatology Research, Vall d'Hebron Research Institute, Universitat Autònoma de Barcelona, 08035 Barcelona, Spain
- Centro Nacional de Análisis Genómico (CNAG), Baldiri Reixac 4, 08028 Barcelona, Spain
- ⁸ Universitat de Barcelona (UB), Barcelona, Spain
- 9 ICREA-Institució Catalana de Recerca i Estudis Avançats, Barcelona, Spain
- * Authors to whom any correspondence should be addressed.

E-mail: smughal@ibecbarcelona.eu, jfernadez@ibecbarcelona.eu and jramon@ibecbarcelona.eu

Keywords: skeletal muscle, chronic fatigue syndrome, Long Covid-19, metabolic adaptation

Supplementary material for this article is available online

Abstract

Myalgic encephalomyelitis/chronic fatigue syndrome (ME/CFS) and Long Covid-19 (LC-19) are complex conditions with no diagnostic markers or consensus on disease progression. Despite extensive research, no *in vitro* model exists to study skeletal muscle wasting, peripheral weakness, or potential therapies. We developed 3D *in vitro* skeletal muscle tissues to map muscle adaptations to patient sera over time. Short exposures (48 H) to patient sera led to a significant reduction in muscle contractile strength. Transcriptomic analysis revealed the upregulation of protein translation, glycolytic enzymes, disturbances in calcium homeostasis, hypertrophy, and mitochondrial hyperfusion. Structural analyses confirmed myotube hypertrophy and elevated mitochondrial oxygen consumption In ME/CFS. While muscles initially adapted by increasing glycolysis, prolonged exposure (96–144 H) caused muscle fragility and weakness, with mitochondria fragmenting into a toroidal conformation. We propose that skeletal muscle tissue in ME/CFS and LC-19 progresses through a hypermetabolic state, leading to severe muscular and mitochondrial deterioration. This is the first study to suggest such transient metabolic adaptation.

1. Introduction

Myalgic encephalomyelitis/chronic fatigue syndrome (ME/CFS), also known as systemic exertion intolerance disease, is a heterogeneous, multisystemic, chronic condition which induces physical and cognitive impairment. Despite the condition affecting approximately 17–24 million people worldwide, its underlying pathomechanism remains poorly understood [1, 2]. ME/CFS predominantly affects women and is characterized by exercise intolerance,

post-exertion (mental, emotional, and physical) symptom exacerbation (PESE), or post-exertional malaise (PEM) [3–5]. Some also report heightened sensitivity to sound, light, and chemicals. Minor activities such as brushing teeth or the anticipation of a hospital visit may trigger severe symptoms, forcing long recuperation times. ME/CFS patients (labeled as CFS in figures), often present with a history of viral or bacterial infection or a predisposition to cancer [6]. Due to non-specific symptoms, patient to patient variability and an overlap of symptomology with

other conditions such as multiple sclerosis (MS), irritable bowel syndrome, fibromyalgia and some types of cancer, misdiagnosis is common. Clinical heterogeneity, is therefore, significant and diagnosis is ultimately dependent on exclusion based on patient-self reporting. At least 20 different diagnoses criteria exist which change frequently and are not unanimously approved till date [7]. Patients diagnosed with COVID-19 also report similar symptoms such as impaired exercise tolerance, extreme fatigue and PESE/PEM after both physical and mental exertion. This has been termed as the post-acute sequelae of COVID-19 or Long COVID-19 (LC-19). Recent studies confirm the various overlapping features between ME/CFS and LC-19 [4, 8, 9].

Peripheral fatigue, a decline in muscle's ability to contract and generate force due to internal causative factors and independent of changes in the brain or spinal cord, is one of the many hallmarks of ME/CFS and LC-19. Patients report high fatiguability which is the tendency of their muscles to tire and lose strength quickly, exercise intolerance and an overall reduced exercise capacity confirmed by clinical studies [3, 4]. Multiple theories exist in contemporary literature attempting to offer various explanations. The Energy Envelope Theory proposes that patients have a limited energy capacity threshold, which when exceeded leads to a worsening of symptoms. This explanation implicates impaired mitochondrial function in ME/CFS patients which compromises their capability for aerobic respiration [10]. The alternative, anaerobic respiration, is less efficient, not only yielding less ATP per glucose molecule but also leading to an accumulation of lactic acid. This results in a decrease in physiological pH, potentially impairing muscle function and inducing fatigue [11]. The push-crash cycle explanation suggests that CFS patients experience a burst of adrenaline and energy causing them to overexert and eventually crash [12]. Studies have also implicated hyperactivation of inflammatory processes and cytokine storms to explain PESE/PEM [2, 8, 13]. Dysfunctional mitochondrial oxidative phosphorylation (OXPHOS) and metabolic disturbances are till date the most widely agreed upon explanations for peripheral fatigue. Other explanations include changes in the composition of systemic factors and the presence of autoantibodies [14–16]. It is evident that investigating metabolic alterations can help in identifying misallocation of energy or metabolic plasticity to manage against stress which could potentially lead to fatigue and oxidative stress [17].

In the last few years, studies on these two idiopathic conditions are predominantly based on blood, muscle biopsies, and cardiopulmonary exercise (ergometry testing) for moderate to severely ill patients [7, 18]. While important, these studies offer limited to no insight on the mechanism of disease advancement but instead, focus on presenting the clinical picture at a timepoint. The major drawback

of these studies is, therefore, an inability to address the issue of progressive muscle wasting which is often wrongfully attributed to only physical inactivity rather than a direct effect of the disease. In patients, understanding this decline in skeletal muscle performance can be difficult due to heavy reliance of current testing methods on biopsies, graded exercise testing and the high probability of false positives at an early stage of disease onset. These approaches also threaten patient safety, comfort, and risk the development of PEM/PESE for those being frequently tested.

Conventional muscle models, such as monolayer cultures are not representative of the complex in vivo skeletal muscle structural and functional features, making them untranslatable [19]. Similarly, data from rodent muscle models has limited reproducibility in humans, with many of the drugs tested in rodent models failing clinical trials [20]. This lack of suitable in vitro models to evaluate and reproduce PEM/PESE presents a critical gap in biomedical research on ME/CFS and LC-19. Recent advances in 3D bioengineered in vitro skeletal micro-physiological systems replicate patient-specific physiological responses and enable the evaluation of pathophysiological responses to circulating systemic factors, such as autoantibodies, circulating cytokines and metabolic or redox toxins present in patient sera. These systems offer a non-invasive testing platform to accurately model conditions without bringing any discomfort to the patient.

Our work aims to understand the pathomechanism of two idiopathic conditions: ME/CFS and LC-19 by using 3D skeletal muscle tissues developed from immortalized human muscle progenitor cells. These mature and well-differentiated tissues were then exposed to sera from ME/CFS, LC-19 and healthy donors for short and long exposures. Exposing tissues to patient sera allowed us to deliver actual systemic insults to muscles in a controlled environment without confounding factors such as physical deconditioning. The contractile profile of the muscle was recorded through electric pulse stimulation (EPS) and transcriptome of treated tissues was analyzed through total RNA sequencing. Subsequently, we quantified mitochondrial morphology and function. Our findings suggest that exposure of 3D skeletal muscle tissues to sera from ME/CFS and LC-19 patients induces significant contractile dysfunction. Both conditions demonstrate mitochondrial dysfunction and transcriptionally adapt distinct responses against sera exposure. ME/CFS muscles, in particular, show elevated oxygen consumption, proton-leak and ATP-linked respiration. Metabolically, both diseases shift muscle energy production towards alternative processes as compensation for mitochondrial defects. Overall, skeletal muscle degeneration in these conditions follows a multi-phasic progression from compensatory adaptation to structural and metabolic collapse driven

by mitochondrial impairment and disrupted protein turnover.

2. Results

2.1. Tissues exhibit contractile weakness at short exposure to patient sera

Impaired power output of skeletal muscles and extreme fatigue is frequently reported by ME/CFS and LC-19 patients [21, 22]. Among the multiple theories existing in contemporary literature, the role of systemic factors in inducing multi-organ complications is also widely accepted. To this end, we fabricated 3D in vitro skeletal muscle tissues from healthy immortalized human myogenic progenitor cells as discussed before [23] to evaluate their contractile performance in response to patient and control sera at short exposure (figure 1(A)). All tissues were welldifferentiated with long, multinucleated myotubes aligned perpendicular to the two pillars prior treatment. The contraction regime included progressively increasing stimulation frequencies to induce both twitch and tetanic contractions (figure 1(B)). The voltage was kept constant at 10 VPP (peak to peak voltage) with 10 s of relaxation after each 10 s stimulation period.

Post 48 h treatment, the tissues exposed to patient sera, henceforth named as diseased tissues, exhibited a significant drop in maximum contractile force (figure 1(C)). Although statistically insignificant, the CFS tissues had a much lower contractile force compared to LC-19 diseased tissues. time in peak (TIP) is the ability of a tissue to maintain peak performance during stimulation. The TIP for diseased treatment groups is significantly shorter compared to the healthy controls (figure 1(D)). Power and velocity of contractions help interpret the ability of a muscle to execute work (figures 1(E) and (F)). These parameters were significantly diminished for all the diseased tissues, albeit more for CFS samples. Consequently, at a higher frequency of 50 Hz, these tissues demonstrated significantly compromised force of contraction as indicated by a much shorter time to drop to 50% relaxation (figure 1(L)). A functional muscle is capable to sustain an increase in its force of contraction proportionally with the stimulus until a certain limit is reached, beyond which depletion of the energy reserves or changes in structural integrity induce impairment [24]. For LC-19 diseased tissues, this limit was reached at a lower stimulating frequency compared to the control and CFS samples. At 25 Hz, a majority of LC-19 tissues appeared to show peak performance following which they could no longer maintain their maximum force against the stimulus (figure 1(k)).

These findings indicate that patient sera not only lowered the overall ability of the muscle to execute work but post peak performance (figure 1(E), (F) and (M)), the tissues experienced weakness and inability

to reach the same performance again, particularly for LC-19 diseased tissues. The model, at short exposure, therefore, replicates muscle weakness and compromised contractile performance frequently experienced by patients. It also hints at the applicability of the push-crash cycle theory on diseased tissues.

2.2. Transcriptomics reveal metabolic plasticity, drop in mitochondrial fission and altered calcium homeostasis at short exposure

To investigate the underlying mechanistic changes in diseased tissues that caused contractile impairment, transcriptomic analyses of the short exposure tissue samples was performed using total RNA sequencing. Interestingly, the multidimensional scaling (MDS) analyses indicated that both ME/CFS and LC-19 treatments clustered together with no significant differentially expressed genes (DEGs) (figure 2(A)). There were, however, several DEGs when ME/CFS and LC-19 tissues were compared to Controls (figures 2(B) and (C)). We further performed gene ontology (GO) enrichment analyses between both patient groups and controls, to identify dysregulated pathways and gene set enrichment anlaysis (GSEA) between ME/CFS and LC-19 to identify any underlying differential biological tendencies. Genes of interest were filtered based on Fold Change and adjusted p-values for both up and downregulated genes (FC $> \pm 1$, and adj p-value < 0.05). Expression of genes with maximum fold change identified by total RNA sequencing was then validated by qRT-PCR. The findings from GO enrichment analyses (figure 6) indicated key changes in muscle structure and contractile function along with cellular metabolism, particularly protein synthesis and translation in ME/CFS while LC-19 samples had an upregulation in mitochondrial structure and function as well as protein translation. The GO enrichment analysis bubble plots provide a comprehensive profile of differential gene expression and regulation patterns (figure 3).

ME/CFS vs control: GO biological processes, cellular components and molecular functions show significant enrichment for upregulated processes particularly in translation, contraction and developmental processes (figures 3(A)–(C)). Prominent upregulated cellular components included ribosomal structures (cytosolic ribosome, large ribosomal subunit) and muscle-related structures such as sarcomere, myofibril, I band, and contractile muscle fiber (figure 3(B)). Upregulated molecular functions in CFS showed a distinct pattern focused on structural components, particularly extracellular matrix (ECM) elements. These include ECM structural constituent conferring tensile strength with high enrichment (FE = 9.48), ECM structural constituent, structural constituent of ribosome, and structural molecule activity (figure 3(C)). According to this GO profile,

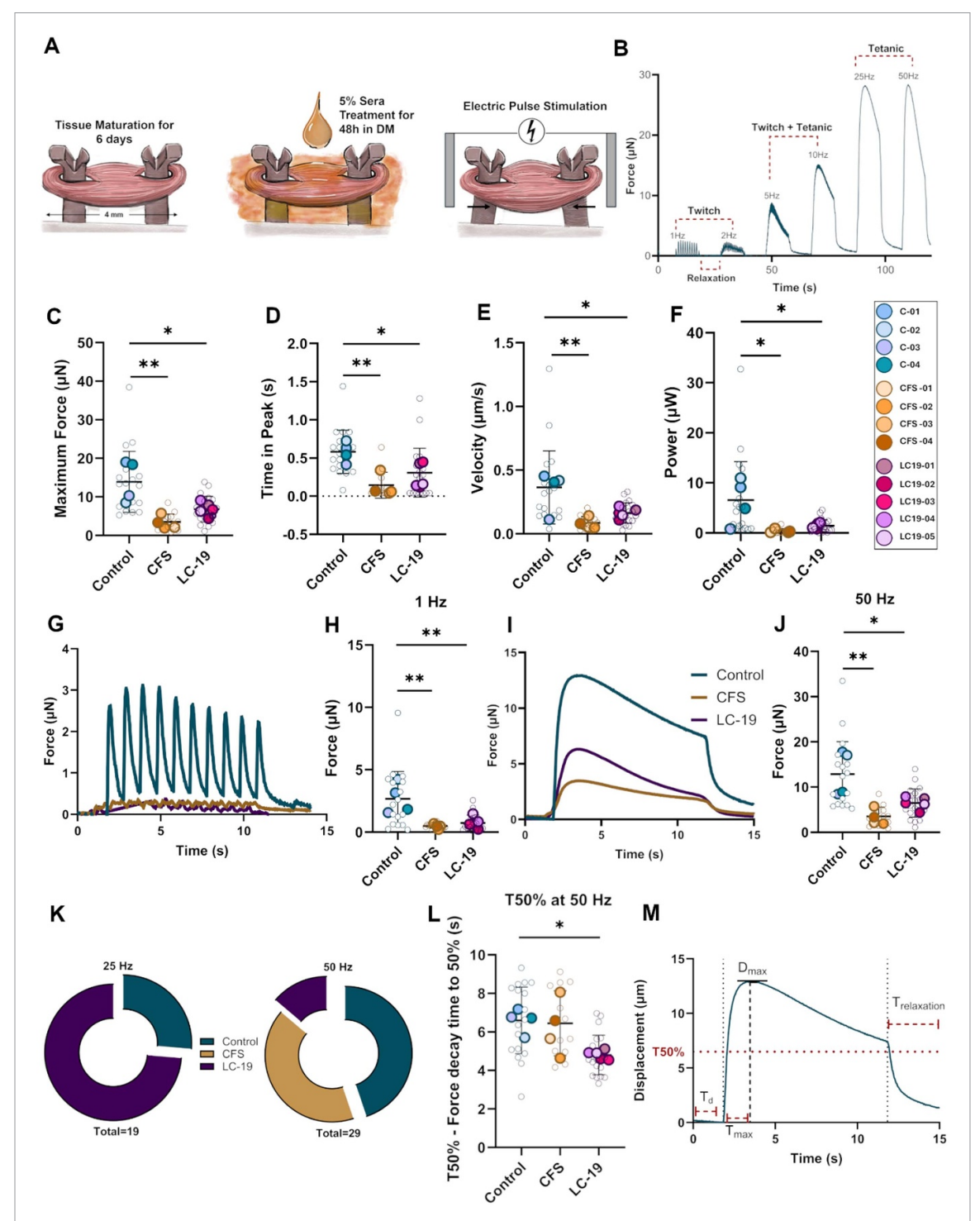


Figure 1. Comparative contractile dynamics post sera treatment for 48 h. (A) Schematic of 3D *in vitro* skeletal muscle tissue maturation and treatment. (B) Stimulation regimen and profile. (C) Maximum contractile force of tissues post treatment. (D) Retention time during maximum contraction, time in peak (TTP). (E) Contractile velocity. (F) Power of contraction (G) twitch spectrum during 1 Hz stimulation. (H) Maximum force during 1 Hz stimulation. (I) Tetanic spectrum during 50 Hz stimulation. (J) Maximum force at 50 Hz. (K) Sample distribution with peak forces at 25 and 50 Hz (L) time taken for the force to drop to 50% of peak value during sustained tetanic stimulation at 50 Hz (T50%). (M) Parameters from tetanic contractions to measure contractile velocity. Statistical analyses: biological replicates: CFS and control, n = 4; LC-19 n = 5 sera from patients or donors. Technical replicates: n = 3–7 tissues per serum. Data show the mean \pm s.d. Statistical analysis: one-way ANOVA with Tukey's post hoc test * $P \le 0.05$; ** $P \le 0.01$.

in ME/CFS skeletal muscle samples there is an upregulation of genes involved in protein translation, ECM, and developmental processes, while genes involved in basic metabolic, transcriptional, and organelle functions are generally downregulated. This could indicate an environment characterized by chronic stress, impaired metabolic activity, and ongoing or maladaptive tissue remodeling.

LC-19 vs control: similar to ME/CFS vs control comparison, a broad downregulation was observed for genes associated with cellular and nuclear functions. In contrast, upregulated terms

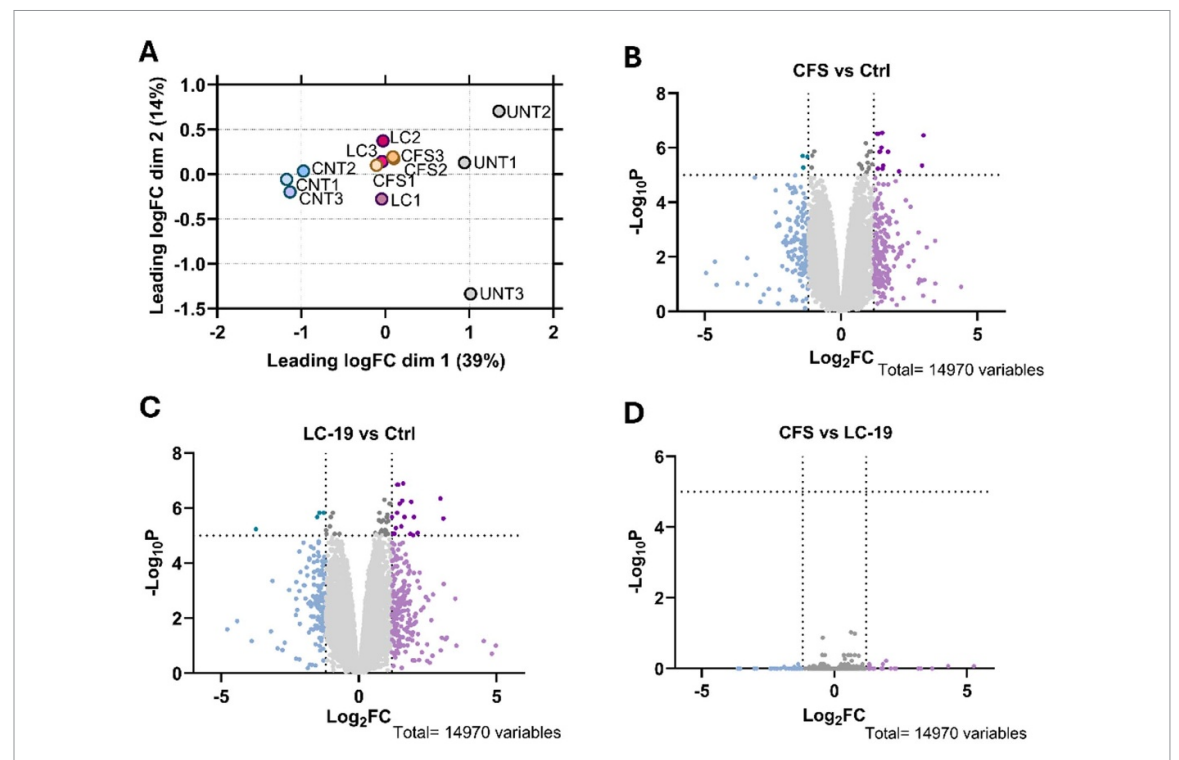


Figure 2. RNA-Seq-MDS and differential expression analyses (A) a multidimensional scaling map for samples. (B) Volcano plot of differentially expressed genes (DEGs) between ME/CFS and control. (C) Volcano plot of differentially expressed genes (DEGs) between LC-19 and control. (D) Volcano plot of differentially expressed genes (DEGs) between ME/CFS and LC-19.

included mitochondrial structures and ribosomal subunits, such as the mitochondrial inner membrane, mitochondrial envelope, and cytosolic ribosome (figures 3(D) and (E)). The molecular function (GO:MF) results further supported this tendency. Downregulated terms include binding activities, such as protein, nucleotide, and anion binding, as well as structural molecule activity with moderate enrichments (figure 3(F)). This pattern suggested a general reduction in the molecular interactions and structural roles. In contrast, the upregulated molecular functions included long-chain fatty acyl-CoA dehydrogenase activity and electron transfer activity. The structural constituent of ribosome and oxidoreduction-driven active transmembrane transporter activity are also upregulated. These findings indicate a pronounced shift in LC-19 tissue toward enhanced mitochondrial fatty acid metabolism, electron transport, and protein synthesis processes.

ME/CFS vs LC-19: although there was a clear absence of significant DEGs between ME/CFS vs LC-19, we were interested to investigate if there were any subtle underlying biological trends or tendencies. Gene set enrichment analysis comparing ME/CFS and LC-19 revealed some interesting differences (figure S1). In ME/CFS, there was significant upregulation of pathways related to ECM organization, including integrin cell surface interactions, collagen degradation, and elastic fiber formation, indicating tissue remodeling and structural changes. Alternatively, compared to LC-19, ME/CFS

also showed strong downregulation of mitochondrial energy production pathways, such as the citric acid (TCA) cycle, respiratory electron transport, and ATP synthesis by chemiosmotic coupling, as well as pathways involved in DNA synthesis and neuronal signaling. These findings highlight a pattern of impaired cellular energy metabolism and enhanced ECM remodeling in ME/CFS compared to LC-19. Our gene set enrichment analysis, further suggested that all compensatory pathways between ME/CFS and LC-19 were upregulated in the latter compared to the former except for cellular response to starvation (figure S2).

Mitochondrial complexes and dynamics:

Gene expression data from RNA sequencing indicated that transcript levels corresponding to Mitochondrial Respiratory Chain complexes were dysregulated in diseased groups, highlighting a compensatory response (figure 4(I)). The upregulation was comparatively more for the LC-19 samples compared to ME/CFS. The same trend was observed for mitochondria encoded genes and those encoded in the nuclear genome. Mitochondrial dynamin related protein 1 (DNM1L) transcript levels were downregulated indicating a drop in mitochondrial fission (figure 3(I)). This observation in conjunction with the upregulation of Mitofusin-2 (MFN2) and SET and MYND domain containing 1 (SMYD1) signposts towards adaptive changes in mitochondrial performance in favor of mitochondrial network

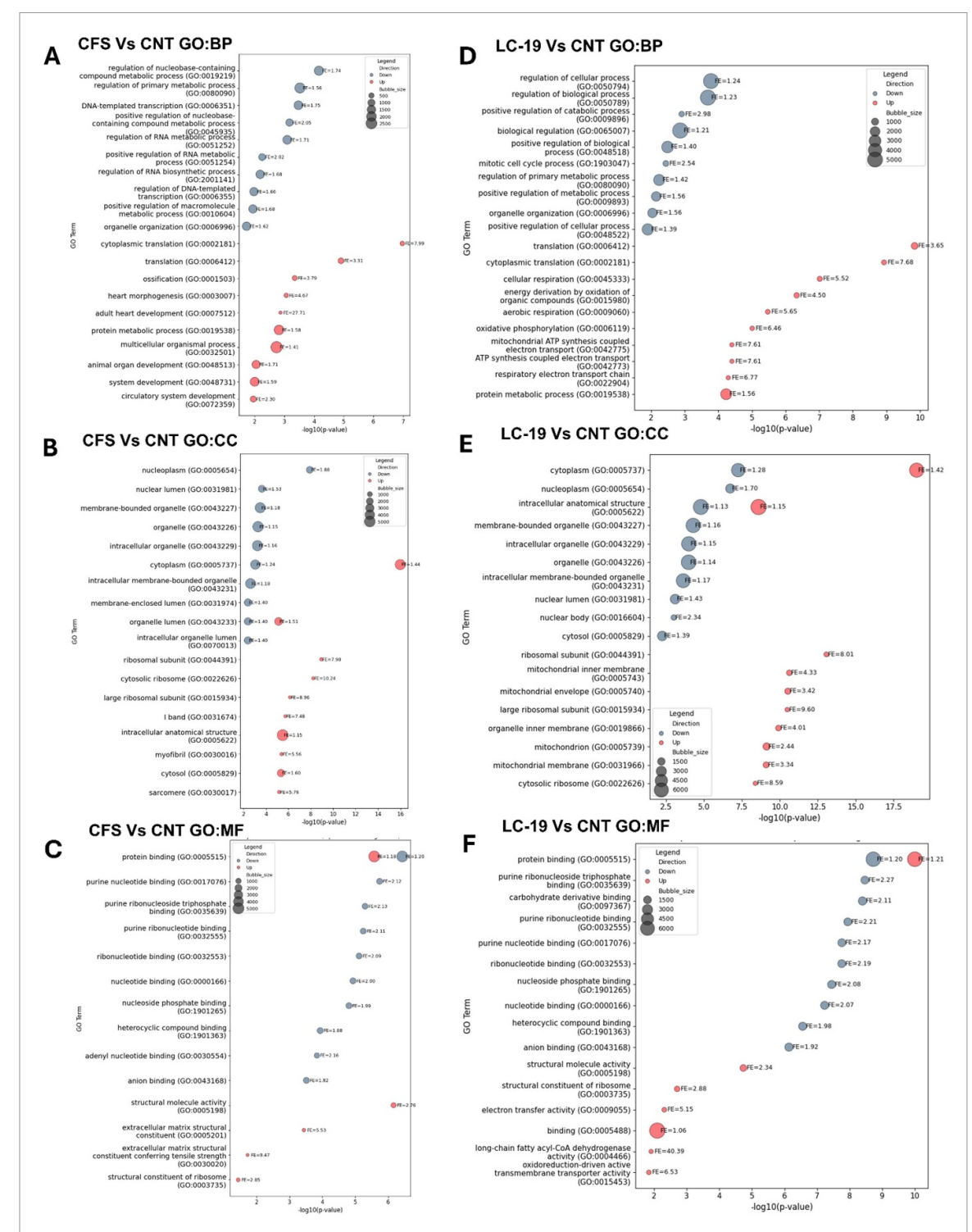


Figure 3. Gene ontology enrichment analysis. (A) CFS vs CNT GO: bioprocesses (B) CFS vs CNT GO: cellular components (C) CFS vs CNT GO: molecular function (D) LC-19 vs CNT GO: bioprocesses (E) LC-19 vs CNT GO: cellular components (F) LC-19 vs CNT GO: molecular function. N = 3 (3 biological replicates and 3 technical replicates per biological replicate were used). Threshold: $\log 2$ FC $\geqslant 1$ and adjusted p value $\leqslant 0.05$.

fusion. Furthermore, upregulation in TCA cycle and glycolytic gene expression for ME/CFS and LC-19 compared to controls indicates cellular adaptation against increased energy demands. In the RNA sequencing analysis, we also observed indication of mitochondrial apoptosis through the upregulated expression of *AIFM1* (apoptosis-inducing factor, mitochondria associated 1) and *ENDOG*

(endonuclease G). *AIFM1* is involved in caspase-independent apoptosis and translocated from the mitochondria to the nucleus upon apoptotic stimulation. It has also been implicated in maintaining mitochondrial OXPHOS [25]. Similar to *AIFM1*, *ENDOG* is also a pro-apoptotic mitochondrial protein. We also observed a downregulation in high temperature requirement A2 which suggested compromised

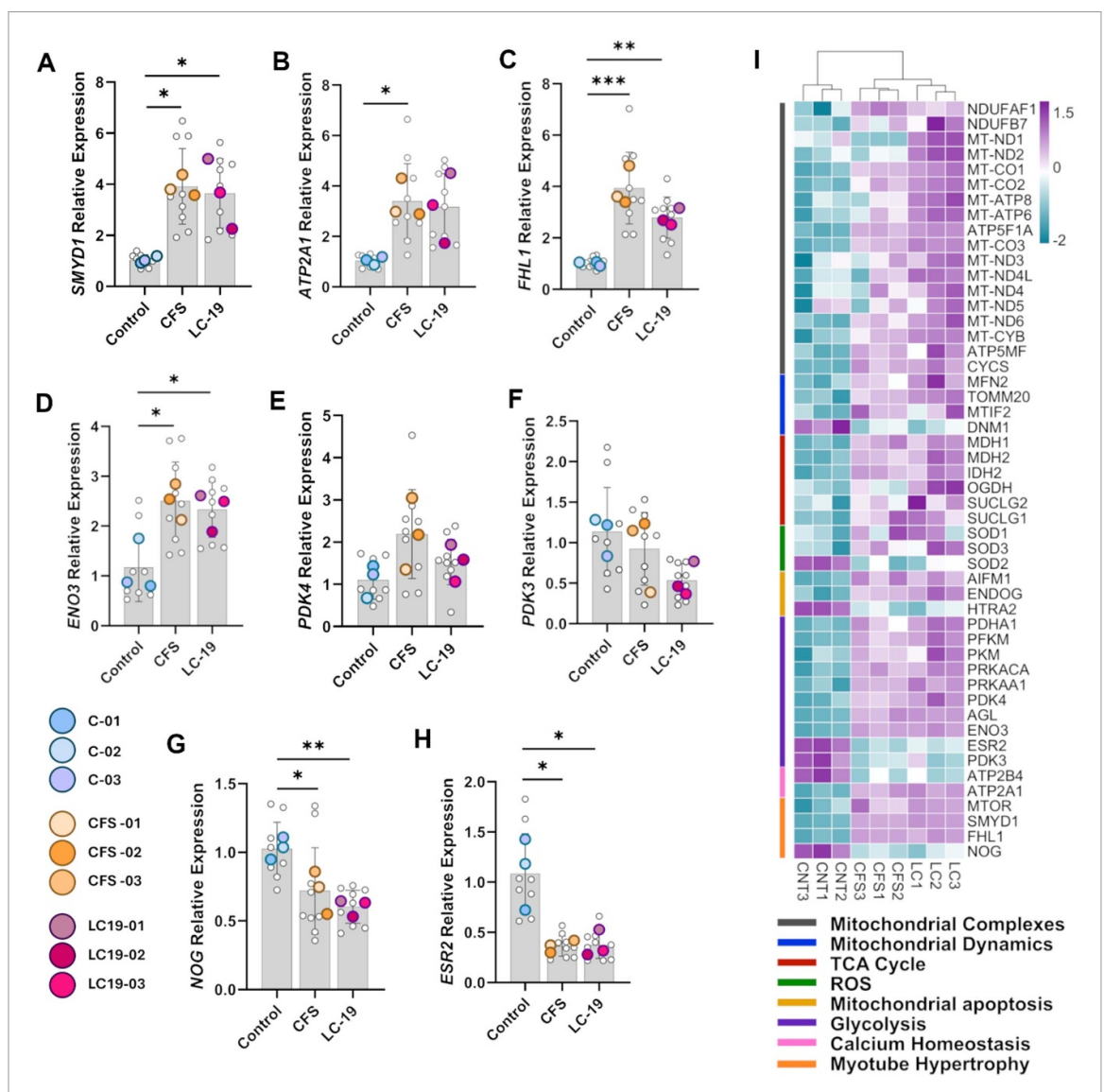


Figure 4. qRT-PCR relative gene expressions of 48 h tissue cohort. (A) *SMYD1* (B) *ATP2A1* (C) *FHL1* (D) *ENO3* (E) *PDK4* (F) *PDK3* (G) *NOG* and (H) *ESR2*. (I) Heatmap of differentially expressed genes from RNASeq. Statistical analyses: biological replicates: ME/CFS and control, n = 3 sera per condition. Technical replicates: n = 4 tissues per serum for all analyses. Data show the mean \pm s.d. Statistical analysis: one-way ANOVA with Tukey's post hoc test * $P \le 0.05$; ** $P \le 0.01$.

mitochondrial protein quality control and accumulation of damaged or misfolded proteins [26].

Validation of DEG expression

A lysine methyl transferase specific for striated muscles, *SMYD1* plays an important role in muscle differentiation and mitochondrial bioenergetics including stabilization of respiratory complexes and cristae formation [27, 28]. It was found to be upregulated in ME/CFS and LC-19 tissues compared to the controls (figures 4(A) and (I)). *SMYD1* gain-offunction has been previously associated with upregulation of mitochondrial respiration as a protective mechanism against injury [27]. Furthermore, the levels of *ATP2A1* which codes for *SERCA1* Ca²⁺-ATPase were also upregulated (figures 4(B) and (I)). Predominantly present in type II fast twitch muscle fibers, this pump is a key regulator of relaxation dynamics of a striated muscle. Found in the sarco-

plasmic reticulum (SR) of muscle cells it pumps the calcium ions from the cytoplasm into the SR, allowing muscle relaxation post contraction and restocking ions for the next contraction [29]. Downregulation in ATP2B4 (calcium ATPase isoform 4) observed in RNA-Seq, (responsible for removing intracellular calcium ions against the large gradients), indicates high calcium sequestering (figure 4(I)). Coupled with an upregulation in ATP2A1 levels, this indicates a disturbance in calcium homeostasis. Increase of calcium sequestering by ATP2A1 in the SR has been related to a disturbance in mitochondrial function and an inducer of fatigue. Increased mitochondrial calcium can trigger the production of ROS through the electron transport chain, particularly the levels of superoxide radicals [30, 31]. Downregulation of SOD2 (superoxide dismutase 2) was observed in diseased tissues, confirming the previously reported data [8]. Coupled with an increase in calcium sequestering, a decrease in SOD2 levels could signal oxidative stress (figure 4(I)).

Four-and-a-half LIM protein 1 (FHL1) has been implicated in inducing myotube hypertrophy [32]. It was found to be overexpressed in the diseased tissues (figures 4(C) and (I)). We also observed an upregulation in transcript levels of glycolytic enzymes such as AGL which codes for glycogen debranching enzyme and ENO3 (beta Enolase) (figures 4(D) and (I)). Both are responsible for regulating the glycolytic pathway and controlling the levels of glucose. Pyruvate dehydrogenase kinase 4 (PDK4) is known to be an important metabolic regulator which increases fatty acid oxidation (figures 4(E) and (I)) [33, 34]. A shift towards fasting-type energy metabolism has been associated with an overexpression of PDK4 [35]. ME/CFS and LC-19 diseased tissues showed an increase in PDK4 gene levels indicating metabolic plasticity under stress conditions warranting a high energy demand. The levels of PDK3, however, were downregulated favoring glucose oxidation (figures 4(F) and (I)). Aberrant PDK levels have previously been 1ssociated with metabolic adaptation in ME/CFS patients [36]. Downregulation of the NOG (noggin) gene has been associated with an increase in bone morphogenetic protein signaling pathway implicated in inducing skeletal muscle hypertrophy which we observed in both LC-19 and ME/CFS treatments (figures 4(G) and (I)) [37]. Estrogen receptor type 2 or ESR2 is known to regulate skeletal muscle growth, regeneration through activation of satellite cells, activating anabolic pathway, and metabolic homeostasis. Loss of ESR2 expression negatively impacts all these processes [38–40] (figures 4(H) and (I)).

2.3. Structural analyses indicates hypertrophy, mitochondrial hyperfusion and elevated oxygen consumption capacity

To further investigate our transcriptomic findings, we undertook structural analyses of myotubes from our short exposure sample cohort and the mitochondria therein. Quantification of myotube diameter was performed by calculating Feret's diameter for individual, transversely cut tubes. The diameter appeared to be enlarged compared to the controls indicating hypertrophic tendencies in diseased ME/CFS and LC-19 tissues (figures 5(A) and (B)). Hypertrophy has been evidenced to be a compensatory response against stress which include self-repair processes [41]. Moreover, quantification of mitochondrial networks showed hyperfusion evidenced by increased mitochondrial branching and mean branch length (figures 3(C)–(E)). Mitochondria had a high aspect ratio and appeared to be hyperbranched in the cytoplasmic space across the length of a myotube as well as close to the nuclei (figure 5(E)). Fusion has

been considered to be a positive response related to mitochondrial health, but evidence suggests that above control levels, excess fusion equates to an increased stress response [42–44]. This coupled with an upregulation in pathways of mitochondrial protein elongation, OXPHOS and energy metabolism observed for ME/CFS and LC-19 in RNA Sequencing (figure 3) confirmed the mitochondrial compensatory response against stress.

We were further intrigued to check mitochondrial functional capacity by the MitoStress Test and observed an increase in the overall oxygen consumption rate (OCR) by the diseased cells compared to the controls (figure 5(F)). The extracellular acidification rate (ECAR) measures the glycolytic process in the cells as a response to treatments. Both the OCR and the EACR were the highest in ME/CFS patients compared to the other two groups (figure 5(G)).

Using this data, we further quantified mitochondrial functions to get deeper insights into respiration and glycolysis after 48 h of patient serum exposure. The basal respiration for ME/CFS samples was substantially higher as was the proton leak post Oligomycin induced blockage of complex V (figures 5(H) and (I)). A corresponding increase in ECAR suggested a significantly higher increase in Glycolysis compared to LC-19 and Control groups (figure 5(I)). A similar trend was observed during the introduction of FCCP, an uncoupler that allows to quantify the maximum OCR that the mitochondria are capable of achieving (figure 5(J)).

Other parameters like ATP-linked respiration, non-mitochondrial respiration and reserve capacity were also slightly upregulated for ME/CFS samples (figures S4(A)-(C)). Non-mitochondrial respiration is attributed to oxygen consumed by nonmitochondrial cellular enzymes and processes, predominantly those that originate from pro-oxidant and pro-inflammatory enzymes such as cyclooxygenases, cytochrome P450s or NADPH oxidases [45]. To investigate this further we calculated the proton production rate (PPR) and the rate of coupled oxygen consumption (oxygen consumption coupled to ATP production) according to the protocol outlined by Mookerjee et al [46], at 48 h of serum treatment, there is an increase in total oxygen consumption, of which the coupled OCR is the highest in tissues treated with ME/CFS (figure S4D) samples followed by the controls and LC-19. To check the dynamics within each treatment we normalized the rates of all mitochondrial processes to basal respirations and confirmed that in LC-19 samples, nonmitochondrial respiration is consuming most of the oxygen (figure S4(F)). However, for ME/CFS samples all processes appear to be upregulated signaling not only a heavy energy burden but also perhaps an attempt to maintain muscle contractile force.

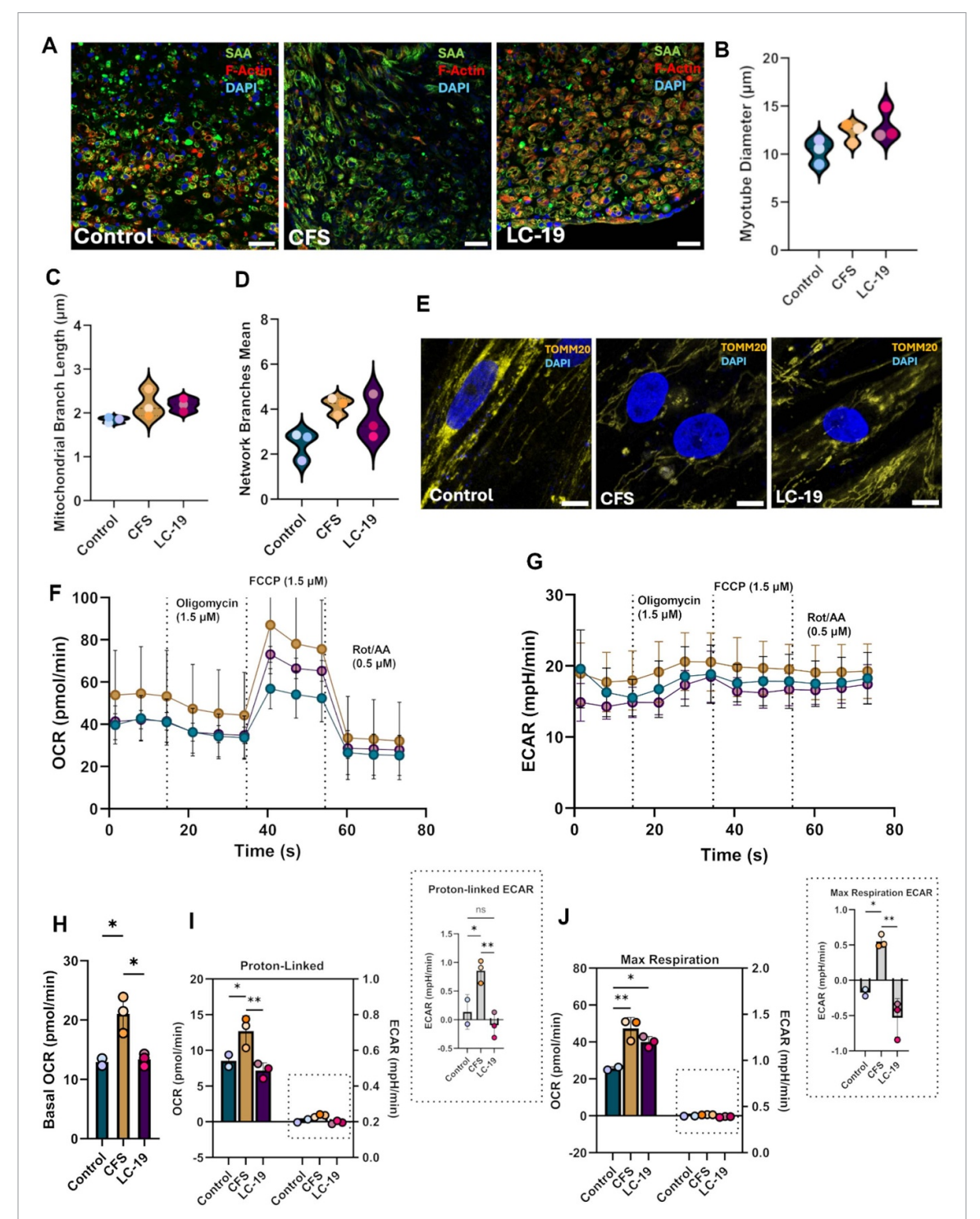


Figure 5. Structural and functional phenotypic validation. (A) Representative confocal images of transverse cross sections stained with an antibody against the mature muscle marker sarcomeric actinin (SAA), phalloidin (F-actin) and DAPI (nuclei). Scale bar: 40 μm. (B) Quantification of myotube diameters n = 3. (C) Quantification of mitochondrial branch length and (D) average network branches n = 3. (E) Representative confocal images of mitochondrial networking stained with inner mitochondrial membrane marker TOMM20 and DAPI. Scale bar = 10 μm (F) profile for oxygen consumption rate (OCR) from the MitoStress test. (G) Extracellular acidification rate (ECAR) profile. (H) Basal oxygen consumption rate (I) proton leak OCR (inset EACR) (J) maximum oxygen consumption rate (inset EACR at maximum respiration). Statistical analyses: biological replicates: CFS and control, n = 3 patients or donors. Technical replicates: n = 4 per serum. Data show the mean \pm s.d. Statistical analysis: one-way ANOVA with Tukey's post hoc test * $P \le 0.05$; ** $P \le 0.01$.

Tissue weakness and fragility increases with exposure along with mitochondrial fragmentation

At 48 h, diseased tissues exhibited a high compensatory response against the systemic stress factors. Based on this data we decided to conduct some initial

tests to determine how the damage manifests and progresses phenotypically during prolonged exposure to patient sera. For this experiment, we used tissues obtained from the same batch of encapsulation to avoid variability in handling and exposed them

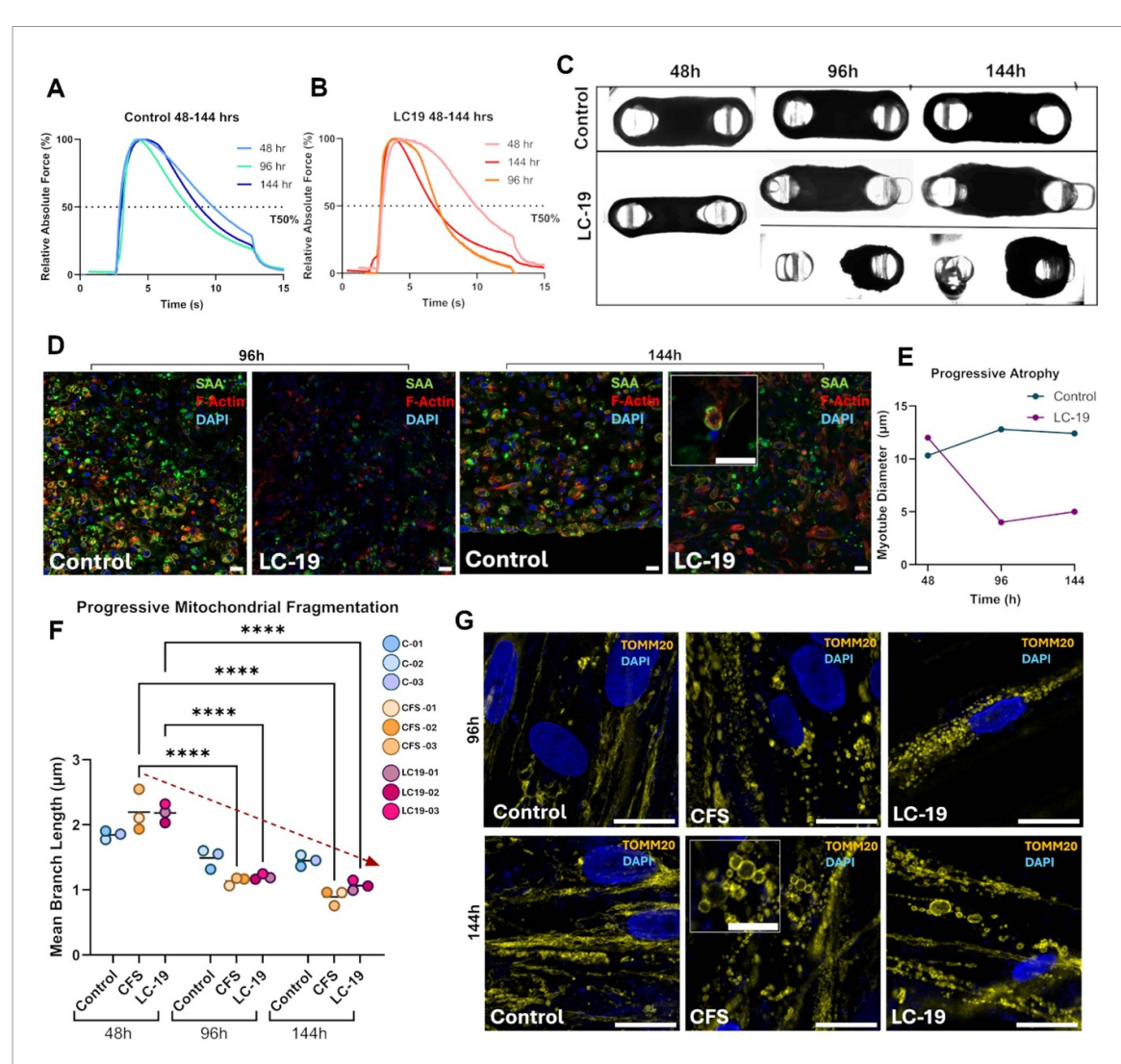


Figure 6. Structural changes over long exposures (A) relative absolute force at 50 Hz for control. The dotted line indicates the time taken for the force to drop to 50% of its peak value under sustained tetanic stimulation of 50 Hz (T50%) (B) relative absolute force at 50 Hz for LC-19 tissues over time. (C) Brightfield images of progressive muscle exposure to control and LC-19 sera. (D) Representative confocal images of transverse cross sections stained with an antibody against the mature muscle marker sarcomeric actinin (SAA), phalloidin (F-actin) and DAPI (nuclei). Scale bar: 20 μ m (10 μ m inset) (E) quantification of myotube diameters overtime (F) quantification of mitochondrial branch length overtime (G) representative confocal images of mitochondrial networking stained with inner mitochondrial membrane marker TOMM20 and DAPI. Scale bar: 10 μ m. Statistical analyses: biological replicates: CFS and control, n = 1. Technical replicates: n = 4 per serum. Data show the mean \pm s.d. Statistical analysis: one-way ANOVA with Tukey's post hoc test * $P \le 0.05$; ** $P \le 0.01$.

to LC-19 and control sera for 48, 96 and 144 h. The diseased tissues were weaker as evidenced by a lower T50% compared to the controls (figure 6(A)). Tissue survival decreased sharply with time for both diseased and control groups, but the decline was two-fold higher for the former than the latter. Brightfield images of the tissues showed distorted LC-19 tissues compared to the controls (figure B). Furthermore, quantification of myotube diameters showed progressive atrophy, with significantly decreased diameters over time (figures 6(D) and (E)). We then analyzed mitochondrial morphology and quantified mitochondrial networks for each time point. Our data indicated a decline in mitochondrial branching and mean branch length. The mitochondria not only assumed the familiar globular geometry observed during fragmentation but also toroidal conformations indicating changes in mitochondrial membrane potential at 144 h of patient serum exposure (figures 6(F) and (G)). The toroidal conformations are typically observed with FCCP administration at high dosages due to depolarization of the mitochondrial membrane, resulting in a drop in mitochondrial membrane potential and uncoupling of mitochondrial OXPHOS and ATP synthesis [47]. These findings confirmed mitochondrial stress induced by systemic stress factors coupled with myotube atrophy at longer exposures. Our results of prolonged exposure to patient sera further warrant investigation due to small sample size but signpost at progressive deterioration of muscle structure, function and mitochondrial energy production, mimicking the conditions observed in patients.

3. Discussion

Research on ME/CFS began when a series of outbreaks of unknown etiology were recorded in 1934. The term 'benign myalgic encephalomyelitis' was first used for patients presenting with malaise, swollen lymph nodes, severe muscular pain, and throat problems. The prefix 'benign' was used to indicate that the condition did not cause mortality. In 1970, however, these reports were declared to be psychosocial phenomena caused by mass hysteria because the patients were commonly female, and the disease lacked physical signs. Over time, research revealed that although it did not cause mortality, the disease was severely disabling and the prefix 'benign' was eventually dropped and ME/CFS was adopted as an umbrella term [48].

Since then, extensive research has revealed physiological and metabolic disturbances that induce multisymptomatic complications in the patients. Contemporary research has implicated the immune system, mitochondrial performance, inflammation induced parenchymal damage of the nervous system, disturbances in amino acid metabolism, local hypoxia, and oxidative damage to induce disease onset [5, 6, 18, 22, 48]. The causative factors were speculated to be either a history of bacterial or viral infections, certain therapies, heightened immune response, a history of cancer and circulating systemic factors. The COVID-19 pandemic brought forward a cohort of LC-19 patients who reported symptoms similar to ME/CFS, warranting a thorough investigation into the overlapping features between the two. In summary, a small fraction of the scientific community is now beginning to appreciate and understand that ME/CFS is an illness, but patients often must wait for years before they can receive a formal diagnosis due to a lack of targeted diagnostic tests. The treatment process is also symptomatic and not definitive.

The aspect of PESE or PEM as mentioned before, is crippling for the patients. Controversial experiments on exercise-based interventions and repetitive biopsy extractions are, therefore, dangerous as they risk exacerbating patient symptoms. Taking advantage of the significant leaps in 3D organ and tissue culture technologies, we decided to investigate the impact of systemic factors on the functional performance and structural integrity of skeletal muscles. To this end, we employed immortalized human muscle progenitor cells to fabricate tissues capable of executing contraction dynamics upon electric stimulation. This not only allowed us to evaluate disease manifestation and progression as close as possible to the in vivo environment but also without causing any distress to the patients. Through this experimental plan, we also sought to answer whether the observed muscular weakness is due to deconditioning or whether certain systemic stress factors in the patient serum are responsible for inducing diminution of physical strength.

To investigate this problem, our tissues were treated with sera from ME/CFS, LC-19 and healthy donors as controls for 48 h initially. Prior to treatment however, we checked cellular viability against the sera at 0.5% and 5% (v/v) concentrations and observed no changes in cellular viability in both 2D and 3D cultures. In our 3D tissues, post-treatment we observed that the maximum contractile strength of ME/CFS and LC-19 treated tissues was severely compromised compared to the controls. A distinguishing feature of the LC-19 tissues was that they reached peak performance at lower frequencies (25 Hz) of our stimulation regimen and could not sustain the same strength at a subsequent higher frequency (50 Hz). This observation coupled with a shorter T50% at 50 Hz confirmed contractile weakness. Previous studies have also shown a lower peak power output in LC-19 patients observed through an exercise test on a cycle ergometer, which our study validated through 3D in vitro skeletal muscle tissues [4, 49]. These findings provide strong evidence against the hypothesis that inactivity is the only cause of muscle wasting in ME/CFS and LC-19 patients. The contractile performance of a skeletal muscle can be diminished due to structural damage, lack of creatine reserves, local hypoxia or insufficient production of ATP due to disturbances in mitochondrial function [50]. The process of OXPHOS produces the maximum amount of ATP by reducing oxygen to sustain cellular bioenergetics [51]. In skeletal muscles, a large proportion of this energy is expended to form Actin-Myosin cross-bridges necessary for contraction. The remainder is used for protein synthesis, glycolysis, ionic balance maintenance and calcium homeostasis. A disturbance or burden on any of these processes may result in an energy imbalance [52]. The observed alteration in contractile force warranted a thorough investigation on the underlying metabolic and bioenergetic processes.

Through RNA sequencing we sought to map the comparative transcriptomic profiles of all the treatment groups. We observed a significant increase in protein translation processes both cytoplasmic and mitochondrial, in ME/CFS and LC-19 cohorts compared to the control. The ME/CFS samples also had an upregulation of extracellular remodeling pathways. Alternatively, LC-19 samples had an upregulation of mitochondrial inner membrane components, ETC, TCA and mitochondrial fatty acid metabolism. These patterns indicated fundamentally different anti-stress mechanisms between two similar conditions of ME/CFS and LC-19.

There was an overall increase in mitochondrial OCR and EACR in the diseased cohort indicating an increased energy demand with a high proton-leak. At 48 h of exposure, it appears that the ME/CFS and LC-19 tissues are at the intersection of mitochondrial damage and unbalanced protein turnover. Furthermore, there was also an increase

in non-mitochondrial oxygen consumption, which meant that of all the oxygen consumed, a significant portion was probably being used by proinflammatory or compensatory processes that levied a high energy burden. ATP also serves as a signaling molecule to recruit cytokines and activate inflammatory processes by binding on purinergic receptors on the immune cells [53]. Multiple studies have reported the infiltration and accumulation of immune cells in skeletal muscles in LC-19 and post-viral ME/CFS [6, 8, 44, 54]. The activation of pro-inflammatory processes can also be strengthened by a high transcriptional expression of antioxidant genes such as SOD1, present in the cytosol and nucleus and SOD3 present in the ECM [55–57]. An intriguing observation, however, was the downregulation of SOD2 which is present in the mitochondria and manages mitochondrial inflammation [8]. The same trend was observed for ME/CFS group as well, indicating oxidative stress as a common denominator between the two as can be observed in figure 4(I). Furthermore, elevated levels of ATP2A1 and downregulated ATP2B4 indicating high sarcoplasmic calcium levels were observed for both diseased groups.

Colosio et al, attributed compromised power output observed in patients to peripheral determinants such as mitochondrial dysfunction [49]. A recent study by Shin et al, evidenced that the SARS-CoV-2 virus enhances mitochondrial metabolism to boost viral propagation [44]. This is accompanied by an increase in mitochondrial fusion. After observing an elevated expression of DNM1 (DRP1) and MFN2 in our RNASeq data, we quantified mitochondrial morphology and detected an increase in mitochondrial fusion despite the large innate heterogeneity in biological replicates. Furthermore, an elevated expression of MTIF2 evidenced an upregulation of mitochondrial protein synthesis and assembly of the OXPHOS complexes. This compensatory upregulation in the expression of mitochondrial genes evidences the presence of a heavy energy burden which required a compensatory metabolic response [58]. The rate of oxygen consumption coupled to ATP synthesis was the lowest in LC-19 cohort, as was the PPR. This indicates that a large part of the consumed oxygen is not being used to maintain contractile strength but instead being invested in an early compensatory adaptation against stress. Mitochondria are double-membered central energy sources that utilize oxygen to produce ATP to sustain cellular bioenergetics. Through the MitoStress test we observed a significant increase in basal mitochondrial respiration as well, indicating a heavy energy burden after 48 h of treatment with sera.

ME/CFS and LC-19 have multiple overlapping features as reported by several studies and confirmed by our RNA Sequencing analyses as well. In the mitochondrial paradigm, however, there do appear to be different trends between the two. Our gene set enrichment analysis suggested that all compensatory

pathways between ME/CFS and LC-19 were upregulated in the latter compared to the former except for cellular response to starvation. For ME/CFS pathways concerning ECM remodeling appeared to be upregulated compared to LC-19. At 48 h of exposure, while sera from ME/CFS and LC-19 appears to condition mitochondria towards hyper consumption of oxygen and metabolism, the ATP produced is not sufficient to maintain contractile performance. We hypothesize this adaptive metabolic reprogramming to not be a complete metabolic switch but instead of a transient nature allowing the cell some buffer time before giving way to atrophy.

Continuing LC-19 serum exposure beyond 48 h induced progressive myotube atrophy evidenced by a reduction in myotube diameter. The tissues contractile strength was compromised and could not maintain strength. A majority of the tissues fractured before they were electrically stimulated to monitor their contractile profiles. Moreover, the mitochondria assumed not only the signature globular geometry observed during fragmentation but also adopted a toroidal conformation indicating altered fusion dynamics, dissipation of mitochondrial membrane potential and cytoskeletal detachment. The toroidal or donut formation precedes fragmentation, which we also observed progressively with time [47].

ME/CFS and LC-19 are complicated multisymptomatic conditions which have severe physical manifestations with a dysregulated energy balance at their core (figure 7). Within a single cell or tissue type various metabolic and homeostatic processes appear to be altered (hyperregulated during short exposures), we speculate that at short exposures, there comes a point in which the biosystem attempts to resist against stress but when the stress is prolonged, the resistance gives in, allowing rapid deterioration. Our research presents the first 3D in vitro model to study performance profiles of ME/CFS and LC-19 patients without distressing them directly. It also provides evidence against two popular misconceptions of hypochondriasis and muscle wasting due to inactivity. While our investigative insights provide pivotal findings regarding disease progression, we do acknowledge the small sample size. This work not only presents a new avenue for ME/CFS and LC-19 research but also posits an important question regarding the nature of systemic factors that are responsible for inducing this stress response. It further highlights the necessity to probe deeper the mechanistic alterations in both the diseases conditions with the minimum amount of confounding variables. Considering the heterogeneity observed in ME/CFS and LC-19 patients (in symptoms, severity, and underlying triggers), it is important to have investigative tools that can reflect this complexity. Traditional approaches often struggle with high variability, especially in smaller patient cohorts, making it hard to detect meaningful trends. Our 3D muscle

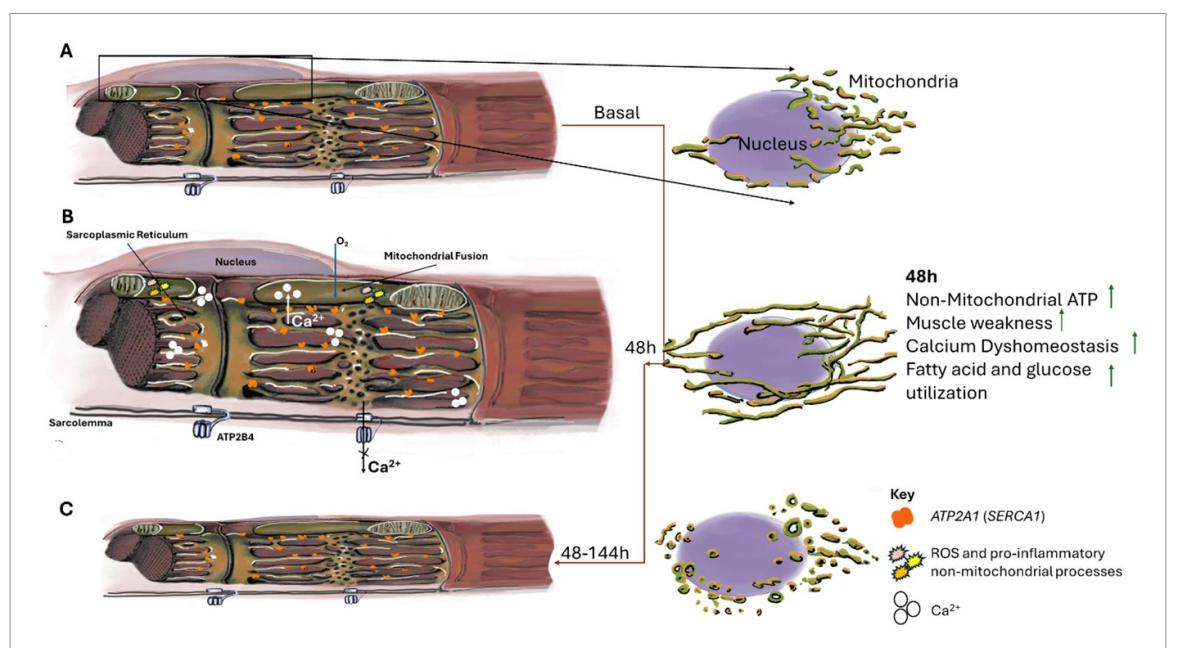


Figure 7. Graphical representation of key findings: (A) baseline structure of a myofiber (B) key changes after 48 h of exposure to ME/CFS and LC-19 sera. (C) Progressive atrophy during long exposure to patient sera.

model offers a way to explore these differences more directly. While we acknowledge the small sample size, the model not only helps understand how the patient serum affects muscle tissue but also presents an opportunity to investigate the personalized effect of patient serum on otherwise healthy tissues.

4. Materials and methods

4.1. Study population

This pilot cohort study was conducted involving individuals with ME/CFS (mean 49.1 ± 3.1 years), 5 long COVID patients (mean age: 48.3 ± 2.4 years) with ongoing post-exertional fatigue for at least 12 months and 4 age-, sex and BMImatched non-fatigued sedentary controls (mean age: 46.7 ± 1.8 years) recruited consecutively between September 2021 and December 2022 from the largest outpatient tertiary referral center in Spain (ME/CFS Clinical Unit, Vall d'Hebron University Hospital, Barcelona, Spain) and Hospital Clinic, Barcelona, Spain. After receiving verbal and written information on the study protocol, all subjects signed informed consent before participation. The study protocol was reviewed and approved by the IRB of Vall d'Hebron University Hospital (reference number: PR/AG 201/2016). All procedures were conducted in accordance with the ethical standards of the board and the 1964 declaration of Helsinki for human research including its later amendments.

4.2. Eligibility criteria

ME/CFS patients were potentially eligible if they were female, aged \geqslant 18 years and had a confirmed diagnosis for ME/CFS by a specialist physician based

on international consensus criteria (2011 ICC), the recommended diagnostic criteria for ME/CFS research purposes [59]. Long COVID patients were eligible for enrollment if they were female, aged ≥ 18 years and, following a confirmed diagnosis of acute COVID-19 infection based on a positive SARS-CoV-2 RT-PCR test on nasal swab during the COVID-19 pandemic, were still suffering from persistent fatigue, unexplained PEM and other core symptoms/signs ≥ 3 months after the acute COVID-19 infection, and met the same clinical case criteria (2011 ICC) for ME/CFS [59]. No-fatigued sedentary donors were eligible if they had neither experienced any post-exertional fatigue/malaise and postacute infection illnesses-associated symptoms/signs nor had been in recent contact with anyone who was infected with SARS-CoV-2 (COVID-19) within 90 d prior to the study, no significant neurological, cardiac, endocrine, or neuroimmune disorders, no alcohol or drug dependence, and did not use daily prescribed medications. All no-fatigued sedentary subjects were recruited through word-of-mouth from the local community and did not meet the case criteria for either ME/CFS or long COVID at the time of enrollment.

All participants were of Caucasian descent, from the same geographical area, and had a sedentary lifestyle at the time of the study. They were subject to stringent exclusion criteria, as previously described [60]. The major exclusion criteria were a relevant previous or current diagnosis of autoimmune disorder, MS, psychosis, major depression disorder, heart disease, hematological disorders, infectious diseases, sleep apnea or metabolic disorders; pregnancy or breast-feeding; smoking habit; strong hormone-related drugs; and preexisting fatigueassociated symptoms or evidence of multiorgan failure that did not meet the case criteria for ME/CFS and long COVID used in this study.

4.3. Blood collection and processing

After a 12 h overnight fasting, 6 ml of peripheral whole blood were collected from each participant between 8:00 a.m. and 10:00 a.m. by a trained phlebotomy nurse (venipuncture from an antecubital vein with a 19-gauge needle) into SST-tubes for serum isolation (BD Vacutainer, Becton Dickenson, Sarstedt, Barcelona, Spain) in the USIC outpatient clinical unit, Vall d'Hebron University Hospital, and Hospital Clinic, Barcelona Spain. One tube was transported and delivered to the local core laboratory within 2 h of collection for routine blood analyses, following standard and recommended procedures. The other blood tube was immediately centrifuged at 2500 rpm for 15 min at 4 °C (Thermo Scientific, Waltham, MA, USA), after which serum specimens was collected and stored in aliquots at −80 °C until further assays. An aliquot of the serum samples was shipped on dry ice to IBEC laboratory for further studies in the 3D 'in vitro' human skeletal muscle model. No serum sample was thawed more than twice.

4.4. Study design

To understand the pathomechanism and develop an *in vitro* model of ME/CFS and LC-19 disease manifestation in a skeletal muscle we adopted a sequential experimentation design. This type of study design helps in understanding idiopathic diseases, where each experiment is planned based on the inferences obtained from a previous experiment. In summary, we made 3D *in vitro* skeletal muscle tissues from immortalized human muscle progenitor cells. After 6 d of differentiation, we treated the mature tissues with 5% patient or control sera for 48, 96 and 144 h and then proceeded with subsequent analyses.

4.5. Fabrication of PDMS platforms

The 3D polydimethylsiloxane (PDMS) platforms were fabricated as published before [61]. Briefly, Master molds were 3D printed using SolusProto (Reify3D, CA, USA) with a Direct Light Projection 3D printer (Solus DLP 3D Printer, Reify3D) at low resolution (80 × 45 mm with a pixel distance of 45 microns). The design was converted to a standard tri-angle language format for printing. After removing all traces of uncured resin by thorough washing and cleaning with ResinAway, the thermo-cured 3D master molds were activated with ozone plasma for 30 s and silanized in a vacuum desiccator with a few drops of trichloro (1H,1H,2H,2H-perfluorooctyl)-silane (PFOTS, Sigma-Aldrich). These 3D printed molds were used to prepare negative molds with

PDMS (5:1), which were then silanized after thorough washing. Post silanization, the negative molds were used to fabricate the final casting molds with PDMS (10:1). After fabrication, all the casting molds were thoroughly washed and dried before using for cell encapsulation [62].

Surface of the final casting platforms was treated with filtered 5% Pluronic F-127 (Sigma-Aldrich) in PBS for atleast 2 h at $4\,^{\circ}$ C to facilitate hydrogel detachment. Pluronic was removed using a filter paper without grazing the bottom of the well. The platforms were stored at $4\,^{\circ}$ C until tissue fabrication.

4.6. Cell culture

Human immortalized muscle precursor cells were obtained from the Institute NeuroMyoGene, Lyon, France [63]. Specifically, cell line control 2-E4 (CNT2-E4) was used with a doubling time of 3.55 d and 99.40% of CD56+ cells. The cells were cultured in skeletal muscle basal growth medium (SMC-GM, C23060, PromoCell) with supplemental mix (C23060, PromoCell), 1% penicillinstreptomycin (10 000 U ml^{-1} , 15140-122, Thermo Fisher Scientific) and 10% fetal bovine serum (10270-106, Thermo Fisher Scientific). For differentiation, the cells were cultured in Dulbecco's modified Eagle medium (DMEM), high glucose, GlutaMAX (Gibco, Thermo Fisher Scientific), 1% v/v penicillin-streptomycin-glutamine (P/S-G, 100×, Gibco, Thermo Fisher Scientific) and 1% v/v insulintransferrin-selenium-ethanolamine supplement (ITS-X, 100×, Gibco, Thermo Fisher Scientific).

4.7. Tissue fabrication

An established protocol in our group was adopted to fabricate functional skeletal muscle tissues [23]. Briefly, for encapsulation, the human muscle precursor cells were trypsinized and resuspended in skeletal muscle growth medium. The cells were encapsulated at a density of 2.5×107 cells ml⁻¹ in 30% v/v Matrigel Growth Factor Reduced basement membrane matrix (Corning), 2 U ml⁻¹ thrombin from human plasma (Sigma-Aldrich) and 4 mg ml⁻¹ fibrinogen from human plasma (Sigma-Aldrich). During hydrogel casting, care was taken to avoid bubbles and cold plasticware was used to prevent polymerization of Matrigel. The mixture was spread as homogenously as possible between the pillars without grazing the surface. After hydrogel introduction all tissues were incubated at 37 °C for 30 min to allow for matrix compaction before adding skeletal muscle growth medium supplemented with 1 mg ml⁻¹ of 6-amino-caproic acid (ACA, SigmaAldrich). The hence formed tissues were allowed to grow for 2 d after which differentiation was initiated for another 6 d by replacing growth medium with differentiation medium (DM) supplemented with 1 mg ml⁻¹ ACA (DM/ACA). Subsequently, half of the DM/ACA was replenished every 2 d to maintain tissue survival.

4.8. Sera treatment on cell monolayers and 3D in vitro skeletal muscle tissues

Muscle constructs with visible structural abnormalities, such as failure to display hydrogel compaction were excluded. Experiments were performed in triplicate on different days and/or in separate batches to ensure reproducibility of our findings. For construct treatment experiments, serum biosamples were randomly assigned to the control or treatment groups. Investigators performing data analysis were blinded to the study hypotheses. After 6 d of differentiation, tissues were treated with 5% (v/v) of serum supplemented in DM/ACA for 48, 96 and 144 h. The serum was diluted from the stock in DM/ACA and added to the respective cultures.

4.9. EPS and force analyses

Post treatment, the bioengineered skeletal muscle tissues were placed in a 12-well plate with custombuilt graphite electrodes connected to a pulse generator (Multifunction Generator WF1974, NF Corporation). An XL S1 cell incubator maintained at 37 °C and 5% CO₂ was used to acquire brightfield images of the plate on top of a Zeiss Axio Observer Z1/7 microscope. The tissues were electrically stimulated to induce both twitch and tetanic contractions. Square monophasic waves of 1–50 Hz were used to generate an electrical field strength of 1 V mm⁻¹ and applied for 10 s. The duty cycle was adjusted as needed to ensure all pulses were 1 ms long. Post analyses the cells were fixed and stored.

Videos were recorded for both pillars at 10X and 39 frames per second during stimulation. Contractile parameters were calculated using pillar displacement from origin during deflection. Force, power and contraction velocity were calculated using the following formulae:

$$F = \frac{6\pi ED^4}{64a^2 (3L - a)}.d$$

$$F = k.d$$

$$V(\max) = \frac{\text{Displacement}(\max)}{TTP + T(\text{delay})}$$

$$P = F.V$$

where: F is force exerted by the tissue; E is the Young's modulus of the PDMS (calculated to be 1.6 ± 0.1 MPa.); D is diameter of the post; a is location of the tissue on the pillar, L is the height of the post; and d is displacement of the pillar. Spring constant k was calculated using the above parameters to be 3.54 N m⁻¹. $V_{\rm (max)}$ is the maximum contractile velocity [64], TTP is the time in seconds to reach

maximum displacement, $T_{(\text{delay})}$ is the delay time in seconds between each stimulation and P is power in μW calculated as shown in figure 1(M).

T50% is the time it takes for the force to drop to 50% of its peak value during sustained tetanic stimulation of 50 Hz. It is calculated as shown in figure 1(M). TIP is the ability of a tissue to maintain peak performance during stimulation or in other words TIP is the duration for which the muscle tissue maintains at least 95% of peak force during a sustained tetanic contraction. TIP has been derived from the force-time plot (figure 1(M))

4.10. RNA extraction, mRNA library preparation and sequencing

Post treatment tissues were flash frozen in liquid nitrogen. Sterilized pestles were used to homogenize the tissues in QIAzol reagent (QIAGEN), and the total RNA was extracted using the miRNeasy Micro Kit (QIAGEN) according to the manufacturer's instructions. Total RNA content was assessed using Nanodrop ND-1000 full spectrum spectrophotometer. Technical replicates were pooled, and the total RNA concentration was adjusted to $100 \text{ ng } \mu l^{-1}$, approximately $1.3 \mu g$ of total RNA per biological replicate or serum. The quantity and quality of the total RNA sample were assessed using the Qubit RNA BR Assay kit (Thermo Fisher Scientific) and the RNA 6000 Nano Bioanalyzer 2100 Assay (Agilent).

RNA-Seq libraries were prepared with the Illumina Stranded Total RNA Prep with Ribo-Zero Plus (Illumina), following the manufacturer's recommendations, starting with 0.5 μg of total RNA as the input material. The final library was validated on an Agilent 2100 Bioanalyzer using the DNA 7500 assay.

The libraries were sequenced on the NovaSeq 6000 (Illumina) with a read length of 2×51 bp following the manufacturer's protocol for dual indexing. Image analysis, base calling, and quality scoring of the run were performed using the manufacturer's software real time analysis (RTA v3.4.4), followed by the generation of FASTQ sequence files

4.11. RNA-Seq data processing and analysis

RNA-Seq reads were mapped against the human reference genome (GRCh38) with STAR 2.7.8a [65] (ref 1) using ENCODE parameters. Genes were quantified with RSEM 1.3.0 [66] using the gencode 44 annotation. Differential expression was performed with limma [67] using the voom transformation of the counts [68]. For the comparisons LC vs CTL and CF vs CTL the DEGs between untreated-CTL were removed. MDS plots was performed with the limma function plotMDS. Functional enrichment for the up and down-regulated genes was performed separately with g:Profiler [69]. Gene set enrichment analysis was done with the pre-ranked list of genes by the limma t moderated statistic, using FGSEA 1.12.0 [70].

4.12. qRT-PCR validation

qRT-PCR was performed as described before [62]. Briefly, 1 μ g of RNA was digested with DNaseI (Invitrogen) and retrotranscribed with SuperScriptII (Invitrogen) using random hexanucleotides. For each biological replicate, qRT-PCR reactions from 10 ng of cDNA were carried out in triplicate using TaqMan probes (applied biosystems). GAPDH, RPLP0 and B2M were used as the endogenous control after comparing their stable expression across different treatment regimens. Thermal cycling was performed using the QuantStudio 5 RT-PCR system (applied biosystems). Relative expression to the endogenous gene and the control group was obtained by the $2 - \Delta \Delta Ct$ method. Pairs of samples were compared using a twotailed unpaired t-test ($\alpha = 0.05$), applying Welch's correction when necessary.

4.13. Cryosectioning and immunoflourescence

After treatments or EPS, the tissues were fixed in 10% formalin (approximately 4% formaldehyde) (Sigma-Aldrich). For transversal sections, tissues were incubated in 30% sucrose solution for 48 h to preserve cellular structure against crystallization. The tissues were then embedded in optimal cutting temperature compound (PolyFreeze, Sigma-Aldrich) in plastic Cryomolds® (VWR, PA, USA) using chilled isopentane. Transverse sections (15 μ m) were obtained by sectioning with a Leica CM1900 cryostat. The sections were transferred to SuperFrost Plus Adhesion slides (Fisher Scientific) and stored at -20 °C.

A PAP pen (ImmEdge, Vector laboratories, CA, USA) was used to encircle tissue sections to minimize waste of antibodies. Sections were rehydrated using PBS and permeabilized with 0.1% Triton X-100 in PBS (PBS-T) for 15 min. Blocking was performed using 0.3% Triton X-100 with 3% Donkey serum in PBS for 30–40 min at room temperature. The tissue sections were then incubated with primary antibodies (see table S1 for details) in blocking buffer at 4 °C overnight.

After overnight incubation, the sections were washed three times with PBS-T and incubated with fluorophore-tagged secondary antibodies and phalloidin (table S1) in blocking buffer for 60 min at room temperature. Post secondary antibody labeling, three PBS-T washes were done, and sections were mounted using VECTASHIELD plus mounting medium with DAPI (Palex). Sections were secured with coverslips and sealed using a transparent enamel.

4.14. Imaging and quantitative morphological analyses

Sections were analyzed using brightfield and confocal imaging with ZEISS Axio Observer Z1/7 and ZEISS LSM800 microscopes, respectively. 20X and higher magnifications were used to procure images from the confocal microscope. After acquisition, images were processed and analyzed using Fiji/ImageJ. To calculate myotube diameter, SAA or phalloidin and DAPI channels were used. Images were binarized and the free hand tool was used to mark the boundary for obtaining Ferret's diameter ($n \ge 50$ per image, at least three images were procured per tissue).

Mitochondrial network analysis in 2D monolayer cultures was performed using mitochondrial network analyzer (StuartLab) plugin in Fiji/ ImageJ. Care was taken to ensure same scale parameters for quantifying images obtained from different magnifications. For each condition, three technical replicates were imaged. Quantification was then performed using atleast three images from each condition relative to the number of nuclei. To evaluate mitochondrial morphology, mitochondrial morphometry macro was used in Fiji/ImageJ (S4).

4.15. MitoStress test—seahorse analysis

Immortalized human muscle progenitor cells were seeded at a density of 4000 cells per well in Seahorse XF HS Mini cell culture plates. Cells were allowed to proliferate until the formation of a uniform monolayer with little to no empty spaces. Once confluent, the growth medium was replaced with DM for 6 d after which 5% serum treated was initiated for 48 h. Once the 48 h treatment was completed, the media was removed, and cells were washed with PBS thrice. The standard assay media was prepared by supplementing Seahorse XF DMEM Media with 10 mM Glucose, 1 mM pyruvate and 2 mM L-Glutamine. Subsequent analyses and treatment steps were followed from the Seahorse XF Cell Mito Stress Test Kit user guide. The concentrations for Oligomycin (1 uM and 2 uM) and FCCP (1.5, 1.8 and 2 uM) were optimized on untreated cells. Final concentrations of the treatments were 1.5 uM of Oligomycin, 1.5 uM of FCCP and 0.5 uM of Rotenone/antimycin A. Post experiment, the cells were lysed in RIPA Buffer for protein quantification and normalization. Detailed equations are presented below (table 1) and a figure schematic explaining drug injections has been shown in figure S6:

Table 1. Equations used in the seahorse analysis.

Parameter	Equation
Non-mitochondrial	Minimum rate
	measurement after
	Rotenone/antimycin A
	injection
Basal respiration	(Last rate measurement
	before first injection)—
	(non-mitochondrial
	respiration rate)
Maximal respiration	(Maximum rate
	measurement after FCCP
	injection)—(non-
	mitochondrial
	respiration)
H+ (Proton) leak	(Minimum rate
	measurement after
	Oligomycin injection)—
	(non-mitochondrial
	respiration)
ATP-linked respiration	(Last rate measurement
	before Oligomycin
	injection)—(minimum rate
	measurement after
	Oligomycin injection)
Spare respiratory capacity	(Maximal
	respiration)—(Basal
	respiration)

4.16. Statistical analyses

Statistical analyses were performed using Prism 9.5 software (GraphPad). All data were tested for normality by using the Shapiro–Wilk test ($P \ge 0.05$). The comparisons between more than two groups were performed by one-way ANOVA. For two groups, unpaired two-tailed parametric Student's t-test with Welch's correction was applied, whereas for non-normal data sets, unpaired two-tailed non-parametric Student's t-test with Mann–Whitney U test was performed. In the case of ANOVA, if a significant trend was observed, Tukey's post hoc tests with 95% confidence interval were applied (P < 0.05)

Data availability statement

All data that support the findings of this study are included within the article (and any supplementary files).

Acknowledgments

We extend gratitude to Dr Benedicte Chazaud from the Institut NeuroMyoGène, Lyon, France, for providing us the human immortalized muscle precursor cells and to the MicroFabSpace and Microscopy Characterization Facility, Unit 7 of Unique Scientific and Technical Infrastructures (ICTS) 'NANBIOSIS' from Networking Biomedical Research Centre-Bioengineering, Biomaterials and

Nanomedicine (CIBER-BBN) at the Institute for Bioengineering of Catalonia (IBEC) for their technical support. We would also like to acknowledge the thorough critique and suggestions on this manuscript presented by Dr Adolfo López de Munain Arregui from the Clinical Neurosciences Unit of Policlínica Gipuzkoa, San Sebastian, Spain and Professor Dr Karl Morten, University of Oxford John Radcliff Hospital, The United Kingdom. Finally, we would also like to express our appreciation to the entire team of Biosensors for Bioengineering group at IBEC for their valuable feedback during the manuscript preparation process.

Funding

This work received financial support from the Ministerio de Ciencia e Innovación (Spain; grant PID2022-136833OB-C22 to J.R.-A.).

S.M. was supported by the FPI predoctoral fellowship from Ministerio de Economía y Competitividad (PRE2020-092676, ayudas para contratos predoctorales para la formación de doctores).

Open Access funding provided by Institute for Bioengineering of Catalonia.

The Spanish Ministry of Science, Innovation and Universities through the 'Severo Ochoa' Program for Centres of Excellence in R&D (CEX2023-001282-S), the CERCA Programme/Generalitat de Catalunya (2021-SGR-01495).

Institutional support to CNAG was provided by the Spanish Ministry of Science and Innovation through the Instituto de Salud Carlos III, and by the Generalitat de Catalunya through the Departament de Salut and the Departament de Recerca i Universitats.

Author contributions

Conceptualization: JR-A, JF-C, SM, GG, JC-M, AE-C.

Methodology: SM, FA-S, AE-C, EC. Investigation: SM, FA-S, GG. Funding acquisition: JR-A.

Project administration: JR-A.

Supervision: JR-A, JF-C. JF-S, JA-M, RS-S.

Writing—original draft: SM.

Writing—review & editing: JR-A, JF-C, GG, JC-M, AE-C.

Conflict of interest

All authors declare no competing interests.

ORCID iDs

Jesús Castro-Marrero © 0000-0002-2481-3052 Juan M Fernández-Costa © 0000-0002-1854-6082 Javier Ramón-Azcón © 0000-0002-3636-8013

References

- [1] Carruthers B M et al 2003 Myalgic encephalomyelitis/chronic fatigue syndrome J. Chronic Fatigue Syndr. 11 7-115
- [2] Cliff J M et al 2019 Cellular immune function in myalgic encephalomyelitis/chronic fatigue syndrome (ME/CFS) Front. Immunol. 10 1–15
- [3] Vøllestad N K and Mengshoel A M 2023 Post-exertional malaise in daily life and experimental exercise models in patients with myalgic encephalomyelitis/chronic fatigue syndrome Front. Physiol. 14 1257557
- [4] Appelman B et al 2024 Muscle abnormalities worsen after post-exertional malaise in long COVID Nat. Commun. 15 17
- [5] Valdez A R et al 2019 Estimating prevalence, demographics, and costs of ME/CFS using large scale medical claims data and machine learning Front. Pediatr. 6 412
- [6] Rasa S, Nora-Krukle Z, Henning N, Eliassen E, Shikova E, Harrer T, Scheibenbogen C, Murovska M and Prusty B K 2018 Chronic viral infections in myalgic encephalomyelitis/chronic fatigue syndrome (ME/CFS) J. Transl. Med. 16 268
- [7] Baker R and Shaw E J 2021 Myalgic Encephalomyelitis (Or Encephalopathy)/chronic Fatigue Syndrome: Diagnosis and Management (National Institute for Health and Care Excellence (NICE))
- [8] Shankar V et al 2024 Oxidative stress is a shared characteristic of ME/CFS and Long COVID J. Immunol. 212 0664 6496
- [9] Komaroff A L and Lipkin W I 2023 ME/CFS and Long COVID share similar symptoms and biological abnormalities: road map to the literature Front. Med. 10 1187163
- [10] Jason L A, Brown M, Brown A, Evans M, Flores S, Grant-Holler E and Sunnquist M 2013 Energy conservation/envelope theory interventions Fatigue: Biomed. Health Behav. 1 27–42
- [11] Sahlin K 2014 Muscle energetics during explosive activities and potential effects of nutrition and training Sports Med. 44 167–73
- [12] Stussman B, Williams A, Snow J, Gavin A, Scott R, Nath A and Walitt B 2020 Characterization of post–exertional Malaise in patients with myalgic encephalomyelitis/chronic fatigue syndrome Front. Neurol. 11 1025
- [13] Klein J et al 2023 Distinguishing features of long COVID identified through immune profiling Nature 623 139–48
- [14] Tomas C, Elson J L, Strassheim V, Newton J L, Walker M, Zhang J and Zhang J 2020 The effect of myalgic encephalomyelitis/chronic fatigue syndrome (ME/CFS) severity on cellular bioenergetic function *PLoS ONE* 15 e0231136
- [15] Smits B, Van Den Heuvel L, Knoop H, Küsters B, Janssen A, Borm G, Bleijenberg G, Rodenburg R and Van Engelen B 2011 Mitochondrial enzymes discriminate between mitochondrial disorders and chronic fatigue syndrome Mitochondrion 11 735–8
- [16] Missailidis D, Annesley S J, Allan C Y, Sanislav O, Lidbury B A, Lewis D P and Fisher P R 2020 An isolated complex V inefficiency and dysregulated mitochondrial function in immortalized lymphocytes from ME/CFS patients Int. J. Mol. Sci. 21 1074
- [17] Walitt B et al 2024 Nath, deep phenotyping of post-infectious myalgic encephalomyelitis/chronic fatigue syndrome Nat. Commun. 15 907
- [18] Nacul L et al 2021 European network on myalgic encephalomyelitis/chronic fatigue syndrome (euromene): expert consensus on the diagnosis, service provision, and care of people with ME/CFS in Europe Medicina 57 510

- [19] Mughal S, López-Muñoz G A, Fernández-Costa J M, Cortés-Reséndiz A, De Chiara F and Ramón-Azcón J 2022 Organs-on-chips: trends and challenges in advanced systems integration Adv. Mater. Interfaces 9 2201618
- [20] van den Berg A, Mummery C L, Passier R and van der Meer A D 2019 Personalised organs-on-chips: functional testing for precision medicine Lab Chip 19 198–205
- [21] Brown A E, Jones D E, Walker M, Newton J L and Philp A 2015 Abnormalities of AMPK activation and glucose uptake in cultured skeletal muscle cells from individuals with chronic fatigue syndrome PLoS ONE 10 e0122982
- [22] Wirth K J and Scheibenbogen C 2021 Pathophysiology of skeletal muscle disturbances in myalgic encephalomyelitis/chronic fatigue syndrome (ME/CFS) J. Transl. Med. 19 1–16
- [23] Fernández-Costa J M, Ortega M A, Rodríguez-Comas J, Lopez-Muñoz G, Yeste J, Mangas-Florencio L, Fernández-González M, Martin-Lasierra E, Tejedera-Villafranca A and Ramon-Azcon J 2023 Training-on-a-chip: a multi-organ device to study the effect of muscle exercise on insulin secretion in vitro Adv. Mater. Technol. 8 2200873
- [24] Angulo J, Assar M E, Álvarez-Bustos A and Rodríguez-Mañas L 2020 Physical activity and exercise: strategies to manage frailty *Redox. Biol.* 35 101513
- [25] Wischhof L, Scifo E, Ehninger D and Bano D 2022 AIFM1 beyond cell death: an overview of this OXPHOS-inducing factor in mitochondrial diseases eBioMedicine 83 104231
- [26] Liu Q, Yan X, Yuan Y, Li R, Zhao Y, Fu J, Wang J and Su J 2024 HTRA2/OMI-mediated mitochondrial quality control alters macrophage polarization affecting systemic chronic inflammation Int. J. Mol. Sci. 25 1577
- [27] Warren J S et al 2018 Histone methyltransferase SMYD1 regulates mitochondrial energetics in the heart Proc. Natl Acad. Sci. USA 115 E7871–80
- [28] Szulik M W et al 2023 SMYD1a protects the heart from ischemic injury by regulating OPA1-mediated cristae remodeling and supercomplex formation Basic Res. Cardiol. 118 20
- [29] Rossi D, Pierantozzi E, Amadsun D O, Buonocore S, Rubino E M and Sorrentino V 2022 The sarcoplasmic reticulum of skeletal muscle cells: a labyrinth of membrane contact sites *Biomolecules* 12 488
- [30] Guo C, Sun L, Chen X and Zhang D 2013 Oxidative stress, mitochondrial damage and neurodegenerative diseases Neural. Regen. Res. 8 2003–14
- [31] Greco M, Munir A, Musarò D, Coppola C and Maffia M 2023 Restoring autophagic function: a case for type 2 diabetes mellitus drug repurposing in Parkinson's disease Front. Neurosci. 17 1244022
- [32] Cowling B S et al 2008 Identification of FHL1 as a regulator of skeletal muscle mass: implications for human myopathy J. Cell Biol. 183 1033–48
- [33] Lim G B 2020 Inhibiting fatty acid oxidation promotes cardiomyocyte proliferation Nat. Rev. Cardiol. 17 266–7
- [34] Dou X et al 2023 PDK4-dependent hypercatabolism and lactate production of senescent cells promotes cancer malignancy Nat. Metab. 5 1887–910
- [35] Pettersen I K N et al 2019 Upregulated PDK4 expression is a sensitive marker of increased fatty acid oxidation Mitochondrion 49 97–110
- [36] Fluge Ø et al 2016 Metabolic profiling indicates impaired pyruvate dehydrogenase function in myalgic encephalopathy/chronic fatigue syndrome JCI Insight 1 1–19
- [37] Winbanks C E et al 2013 The bone morphogenetic protein axis is a positive regulator of skeletal muscle mass J. Cell Biol. 203 345–57
- [38] Seko D, Fujita R, Kitajima Y, Nakamura K, Imai Y and Ono Y 2020 Estrogen receptor β controls muscle growth and regeneration in young female mice Stem Cell Rep. 15 577–86
- [39] Hevener A L, Zhou Z, Drew B G and Ribas V 2017 In sex and gender factors affecting metabolic homeostasis, diabetes and

- obesity Advances in Experimental Medicine and Biology vol 1043, ed F Mauvais-Jarvis (Springer) pp 257–84
- [40] Gregorio K C R, Laurindo C P and Machado U F 2021 Estrogen and glycemic homeostasis: the fundamental role of nuclear estrogen receptors ESR1/ESR2 in glucose transporter GLUT4 regulation Cells 10 99
- [41] Li J et al 2024 An engineered anisotropic skeletal muscle organoid-on-a-chip for deciphering muscle response under intermittent hypoxia Adv. Funct. Mater. 34 2401564
- [42] Yao C-H, Wang R, Wang Y, Kung C-P, Weber J D and Patti G J 2019 Mitochondrial fusion supports increased oxidative phosphorylation during cell proliferation *Elife* 8 e41351
- [43] Bernhardt D, Müller M, Reichert A S and Osiewacz H D 2015 Simultaneous impairment of mitochondrial fission and fusion reduces mitophagy and shortens replicative lifespan Sci. Rep. 5 1–9
- [44] Shin H J et al 2024 SARS-CoV-2 aberrantly elevates mitochondrial bioenergetics to induce robust virus propagation Signal Transduct. Target. Ther. 9 125
- [45] Chacko B K et al 2014 The bioenergetic health index: a new concept in mitochondrial translational research Clin. Sci. (Lond) 127 367–73
- [46] Mookerjee S A, Gerencser A A, Nicholls D G and Brand M D 2017 Quantifying intracellular rates of glycolytic and oxidative ATP production and consumption using extracellular flux measurements J. Biol. Chem. 292 7189–207
- [47] Liu X and Hajnóczky G 2011 Altered fusion dynamics underlie unique morphological changes in mitochondria during hypoxia—reoxygenation stress Cell Death Differ. 18 1561–72
- [48] 2015 Beyond Myalgic Encephalomyelitis/chronic Fatigue Syndrome: Redefining an Illness (National Academies Press)
- [49] Colosio M et al 2023 Structural and functional impairments of skeletal muscle in patients with postacute sequelae of SARS-CoV-2 infection J. Appl. Physiol. 135 902–17
- [50] Chen T-H, Koh K-Y, Lin K M-C and Chou C-K 2022 Mitochondrial dysfunction as an underlying cause of skeletal muscle disorders *Int. J. Mol. Sci.* 23 12926
- [51] Cooper G M 2000 The Cell: A Molecular Approach 2nd edn (ASM Press)
- [52] Kuo I Y and Ehrlich B E 2015 Signaling in muscle contraction Cold Spring Harb. Perspect. Biol. 7 a006023
- [53] Ai Y, Wang H, Liu L, Qi Y, Tang S, Tang J and Chen N 2023 Purine and purinergic receptors in health and disease MedComm 4 e359
- [54] Pietrangelo T et al 2024 Myalgic encephalomyelitis/chronic fatigue syndrome from current evidence to new diagnostic perspectives through skeletal muscle and metabolic disturbances Acta. Physiol. 240 e14122
- [55] Fukai T and Ushio-Fukai M 2011 Superoxide dismutases: role in redox signaling, vascular function, and diseases Antioxid. Redox Signal. 15 1583–606
- [56] Zheng M, Liu Y, Zhang G, Yang Z, Xu W and Chen Q 2023 The applications and mechanisms of superoxide dismutase in medicine, food, and cosmetics *Antioxidants* 12 1675
- [57] Jomova K, Raptova R, Alomar S Y, Alwasel S H, Nepovimova E, Kuca K and Valko M 2023 Reactive oxygen

- species, toxicity, oxidative stress, and antioxidants: chronic diseases and aging *Arch. Toxicol.* **97** 2499–574
- [58] Havlíčková Karbanová V, Čížková Vrbacká A, Hejzlarová K, Nůsková H, Stránecký V, Potocká A, Kmoch S and Houštěk J 2012 Compensatory upregulation of respiratory chain complexes III and IV in isolated deficiency of ATP synthase due to TMEM70 mutation *Biochim. Biophys. Acta Bioenerg.* 1817 1037–43
- [59] Carruthers B M et al 2011 Myalgic encephalomyelitis: international consensus criteria J. Internal Med. 270 327–38
- [60] Cambras T, Zerón-Rugerio M F, Díez-Noguera A, Zaragozá M C, Domingo J C, Sanmartin-Sentañes R, Alegre-Martin J and Castro-Marrero J 2023 Skin temperature circadian rhythms and dysautonomia in myalgic encephalomyelitis/chronic fatigue syndrome: the role of endothelin-1 in the vascular tone dysregulation *Int. J. Mol. Sci.* 24 4835
- [61] Fernández-Costa J M et al 2022 Training-on-a-Chip: a multi-organ device to study the effect of muscle exercise on insulin secretion in vitro Adv. Mater. Technol. 8 2200873
- [62] Mughal S, Sabater-Arcis M, Artero R, Ramón-Azcón J and Fernández-Costa J M 2024 Taurine activates the AKT-mTOR axis to restore muscle mass and contractile strength in human 3D in vitro models of steroid myopathy Dis. Models Mech. 17 dmm050540
- [63] Massenet J, Gitiaux C, Magnan M, Cuvellier S, Hubas A, Nusbaum P, Dilworth F J, Desguerre I and Chazaud B 2020 Derivation and characterization of immortalized human muscle satellite cell clones from muscular dystrophy patients and healthy individuals *Cells* 9 1780
- [64] Loturco I, Pereira L A, Kobal R, Kitamura K, Ramírez-Campillo R, Zanetti V, Abad C C C and Nakamura F Y 2016 Muscle contraction velocity: a suitable approach to analyze the functional adaptations in elite soccer players J. Sports Sci. Med. 15 483–91
- [65] Dobin A, Davis C A, Schlesinger F, Drenkow J, Zaleski C, Jha S, Batut P, Chaisson M and Gingeras T R 2013 STAR: ultrafast universal RNA-Seq aligner *Bioinformatics* 29 15–21
- [66] Li B and Dewey C N 2011 RSEM: accurate transcript quantification from RNA-Seq data with or without a reference genome BMC Bioinf. 12 323
- [67] Ritchie M E, Phipson B, Wu D, Hu Y, Law C W, Shi W and Smyth G K 2015 Limma powers differential expression analyses for RNA-sequencing and microarray studies *Nucleic Acids Res.* 43 e47
- [68] Law C W, Chen Y, Shi W and Smyth G K 2014 voom: precision weights unlock linear model analysis tools for RNA-seq read counts *Genome Biol.* 15 R29
- [69] Kolberg L, Raudvere U, Kuzmin I, Adler P, Vilo J and Peterson H 2023 g: profiler—interoperable web service for functional enrichment analysis and gene identifier mapping (2023 update) Nucleic Acids Res. 51 W207–12
- [70] Korotkevich G, Sukhov V, Budin N, Shpak B, Artyomov M N and Sergushichev A 2021 Fast gene set enrichment analysis bioRxiv Preprint (https://doi.org/10.1101/060012) (posted online 01 February 2021)